Measurement of the $e^+e^- \rightarrow$ ZZ Production Cross Section at Centre-of-mass Energies of 183 and 189 GeV

ALEPH Collaboration

Abstract

The $e^+e^- \rightarrow$ ZZ cross section at $\sqrt{s} = 182.7$ and 188.6 GeV has been measured using the ALEPH detector. The analysis covers all of the visible ZZ final states and yields cross section measurements of

$$\sigma_{ZZ}(182.7\text{ GeV}) = 0.11 \pm {}^{0.16}_{0.11}\,(\text{stat.}) \pm 0.04\,(\text{syst.})\,\text{pb}$$

and

$$\sigma_{ZZ}(188.6\text{ GeV}) = 0.67 \pm 0.13\,(\text{stat.}) \pm 0.04\,(\text{syst.})\,\text{pb},$$

consistent with the Standard Model expectations.

The ALEPH Collaboration

R. Barate, D. Decamp, P. Ghez, C. Goy, S. Jezequel, J.-P. Lees, F. Martin, E. Merle, M.-N. Minard, B. Pietrzyk

Laboratoire de Physique des Particules (LAPP), IN²P³-CNRS, F-74019 Annecy-le-Vieux Cedex, France

R. Alemany, S. Bravo, M.P. Casado, M. Chmeissani, J.M. Crespo, E. Fernandez, M. Fernandez-Bosman, Ll. Garrido,[15] E. Graugès, A. Juste, M. Martinez, G. Merino, R. Miquel, Ll.M. Mir, P. Morawitz, A. Pacheco, I. Riu, H. Ruiz

Institut de Física d'Altes Energies, Universitat Autònoma de Barcelona, 08193 Bellaterra (Barcelona), E-Spain[7]

A. Colaleo, D. Creanza, M. de Palma, G. Iaselli, G. Maggi, M. Maggi, S. Nuzzo, A. Ranieri, G. Raso, F. Ruggieri, G. Selvaggi, L. Silvestris, P. Tempesta, A. Tricomi,[3] G. Zito

Dipartimento di Fisica, INFN Sezione di Bari, I-70126 Bari, Italy

X. Huang, J. Lin, Q. Ouyang, T. Wang, Y. Xie, R. Xu, S. Xue, J. Zhang, L. Zhang, W. Zhao

Institute of High-Energy Physics, Academia Sinica, Beijing, The People's Republic of China[8]

D. Abbaneo, G. Boix,[6] O. Buchmüller, M. Cattaneo, F. Cerutti, V. Ciulli, G. Davies, G. Dissertori, H. Drevermann, R.W. Forty, M. Frank, F. Gianotti, T.C. Greening, A.W. Halley, J.B. Hansen, J. Harvey, P. Janot, B. Jost, I. Lehraus, O. Leroy, P. Maley, P. Mato, A. Minten, A. Moutoussi, F. Ranjard, L. Rolandi, D. Schlatter, M. Schmitt,[20] O. Schneider,[2] P. Spagnolo, W. Tejessy, F. Teubert, E. Tournefier, A.E. Wright

European Laboratory for Particle Physics (CERN), CH-1211 Geneva 23, Switzerland

Z. Ajaltouni, F. Badaud G. Chazelle, O. Deschamps, S. Dessagne, A. Falvard, C. Ferdi, P. Gay, C. Guicheney, P. Henrard, J. Jousset, B. Michel, S. Monteil, J-C. Montret, D. Pallin, P. Perret, F. Podlyski

Laboratoire de Physique Corpusculaire, Université Blaise Pascal, IN²P³-CNRS, Clermont-Ferrand, F-63177 Aubière, France

J.D. Hansen, J.R. Hansen, P.H. Hansen, B.S. Nilsson, B. Rensch, A. Wäänänen

Niels Bohr Institute, 2100 Copenhagen, DK-Denmark[9]

G. Daskalakis, A. Kyriakis, C. Markou, E. Simopoulou, A. Vayaki

Nuclear Research Center Demokritos (NRCD), GR-15310 Attiki, Greece

A. Blondel, J.-C. Brient, F. Machefert, A. Rougé, M. Swynghedauw, R. Tanaka, A. Valassi,[23] H. Videau

Laboratoire de Physique Nucléaire et des Hautes Energies, Ecole Polytechnique, IN²P³-CNRS, F-91128 Palaiseau Cedex, France

E. Focardi, G. Parrini, K. Zachariadou

Dipartimento di Fisica, Università di Firenze, INFN Sezione di Firenze, I-50125 Firenze, Italy

M. Corden, C. Georgiopoulos

Supercomputer Computations Research Institute, Florida State University, Tallahassee, FL 32306-4052, USA [13,14]

A. Antonelli, G. Bencivenni, G. Bologna,[4] F. Bossi, P. Campana, G. Capon, V. Chiarella, P. Laurelli, G. Mannocchi,[1,5] F. Murtas, G.P. Murtas, L. Passalacqua, M. Pepe-Altarelli

Laboratori Nazionali dell'INFN (LNF-INFN), I-00044 Frascati, Italy

M. Chalmers, L. Curtis, J.G. Lynch, P. Negus, V. O'Shea, B. Raeven, C. Raine, D. Smith, P. Teixeira-

Dias, A.S. Thompson, J.J. Ward

  Department of Physics and Astronomy, University of Glasgow, Glasgow G12 8QQ,United Kingdom[10]

R. Cavanaugh, S. Dhamotharan, C. Geweniger,[1] P. Hanke, V. Hepp, E.E. Kluge, A. Putzer, K. Tittel, S. Werner,[19] M. Wunsch[19]

  Institut für Hochenergiephysik, Universität Heidelberg, D-69120 Heidelberg, Germany[16]

R. Beuselinck, D.M. Binnie, W. Cameron, P.J. Dornan,[1] M. Girone, S. Goodsir, N. Marinelli, E.B. Martin, J. Nash, J. Nowell, H. Przysieezniak,[1] A. Sciabà, J.K. Sedgbeer, E. Thomson, M.D. Williams

  Department of Physics, Imperial College, London SW7 2BZ, United Kingdom[10]

V.M. Ghete, P. Girtler, E. Kneringer, D. Kuhn, G. Rudolph

  Institut für Experimentalphysik, Universität Innsbruck, A-6020 Innsbruck, Austria[18]

C.K. Bowdery, P.G. Buck, G. Ellis, A.J. Finch, F. Foster, G. Hughes, R.W.L. Jones, N.A. Robertson, M. Smizanska, M.I. Williams

  Department of Physics, University of Lancaster, Lancaster LA1 4YB, United Kingdom[10]

I. Giehl, F. Hölldorfer, K. Jakobs, K. Kleinknecht, M. Kröcker, A.-S. Müller, H.-A. Nürnberger, G. Quast, B. Renk, E. Rohne, H.-G. Sander, S. Schmeling, H. Wachsmuth C. Zeitnitz, T. Ziegler

  Institut für Physik, Universität Mainz, D-55099 Mainz, Germany[16]

J.J. Aubert, A. Bonissent, J. Carr, P. Coyle, A. Ealet, D. Fouchez, A. Tilquin
  Centre de Physique des Particules, Faculté des Sciences de Luminy, IN²P³-CNRS, F-13288 Marseille, France

M. Aleppo, M. Antonelli, S. Gilardoni, F. Ragusa
  Dipartimento di Fisica, Università di Milano e INFN Sezione di Milano, I-20133 Milano, Italy.

V. Büscher, H. Dietl, G. Ganis, K. Hüttmann, G. Lütjens, C. Mannert, W. Männer, H.-G. Moser, S. Schael, R. Settles, H. Seywerd, H. Stenzel, W. Wiedenmann, G. Wolf

  Max-Planck-Institut für Physik, Werner-Heisenberg-Institut, D-80805 München, Germany[16]

P. Azzurri, J. Boucrot, O. Callot, S. Chen, M. Davier, L. Duflot, J.-F. Grivaz, Ph. Heusse, A. Jacholkowska,[1] M. Kado, J. Lefrançois, L. Serin, J.-J. Veillet, I. Videau,[1] J.-B. de Vivie de Régie, D. Zerwas
  Laboratoire de l'Accélérateur Linéaire, Université de Paris-Sud, IN²P³-CNRS, F-91898 Orsay Cedex, France

G. Bagliesi, T. Boccali, C. Bozzi,[12] G. Calderini, R. Dell'Orso, I. Ferrante, A. Giassi, A. Gregorio, F. Ligabue, P.S. Marrocchesi, A. Messineo, F. Palla, G. Rizzo, G. Sanguinetti, G. Sguazzoni, R. Tenchini, A. Venturi, P.G. Verdini
  Dipartimento di Fisica dell'Università, INFN Sezione di Pisa, e Scuola Normale Superiore, I-56010 Pisa, Italy

G.A. Blair, J. Coles, G. Cowan, M.G. Green, D.E. Hutchcroft, L.T. Jones, T. Medcalf, J.A. Strong
  Department of Physics, Royal Holloway & Bedford New College, University of London, Surrey TW20 OEX, United Kingdom[10]

D.R. Botterill, R.W. Clifft, T.R. Edgecock, P.R. Norton, J.C. Thompson, I.R. Tomalin
  Particle Physics Dept., Rutherford Appleton Laboratory, Chilton, Didcot, Oxon OX11 OQX, United Kingdom[10]

B. Bloch-Devaux, P. Colas, B. Fabbro, G. Faïf, E. Lançon, M.-C. Lemaire, E. Locci, P. Perez, J. Rander, J.-F. Renardy, A. Rosowsky, P. Seager,[24] A. Trabelsi,[21] B. Tuchming, B. Vallage
  CEA, DAPNIA/Service de Physique des Particules, CE-Saclay, F-91191 Gif-sur-Yvette Cedex, France[17]

S.N. Black, J.H. Dann, C. Loomis, H.Y. Kim, N. Konstantinidis, A.M. Litke, M.A. McNeil, G. Taylor
  Institute for Particle Physics, University of California at Santa Cruz, Santa Cruz, CA 95064, USA[22]

C.N. Booth, S. Cartwright, F. Combley, P.N. Hodgson, M. Lehto, L.F. Thompson

Department of Physics, University of Sheffield, Sheffield S3 7RH, United Kingdom[10]

K. Affholderbach, A. Böhrer, S. Brandt, C. Grupen, J. Hess, A. Misiejuk, G. Prange, U. Sieler

Fachbereich Physik, Universität Siegen, D-57068 Siegen, Germany[16]

G. Giannini, B. Gobbo

Dipartimento di Fisica, Università di Trieste e INFN Sezione di Trieste, I-34127 Trieste, Italy

J. Putz, J. Rothberg, S. Wasserbaech, R.W. Williams

Experimental Elementary Particle Physics, University of Washington, WA 98195 Seattle, U.S.A.

S.R. Armstrong, P. Elmer, D.P.S. Ferguson, Y. Gao, S. González, O.J. Hayes, H. Hu, S. Jin, J. Kile, P.A. McNamara III, J. Nielsen, W. Orejudos, Y.B. Pan, Y. Saadi, I.J. Scott, J. Walsh, J.H. von Wimmersperg-Toeller, Sau Lan Wu, X. Wu, G. Zobernig

Department of Physics, University of Wisconsin, Madison, WI 53706, USA[11]

1   Introduction

The successful operation of LEP at and above the ZZ threshold in 1997 and 1998 allows observation of a sizable number of pair-produced resonant Z bosons. Within the Standard Model, the process $e^+e^- \rightarrow$ ZZ proceeds via the two $\mathcal{NC2}$ diagrams which involve the t-channel exchange of an electron (see Figure 1). A measurement of this process, the dominant irreducible background for Higgs boson searches at LEP, tests the rates predicted by the Standard Model.

This letter describes a measurement of the ZZ $\mathcal{NC2}$ cross section at a centre-of-mass energy of 188.6 GeV using the ALEPH detector. It begins with a description of the detector and data samples, continues with a description of the event selections for the various final states, and concludes with the measured cross section. Application of the same analysis to the 1997 ALEPH data also yields a measurement of the cross section at $\sqrt{s} =$182.7 GeV.

2   ALEPH Detector

This section briefly describes the most salient features of the ALEPH detector; detailed descriptions of the detector and its performance can be found elsewhere [1, 2].

ALEPH is a cylindrically symmetric detector with its axis coincident with the beam axis. The three innermost detectors—a silicon microstrip detector, the inner tracking chamber, and the time-projection chamber (TPC)—measure the momentum of charged particles. With a 1.5 T axial magnetic field provided by a superconducting solenoidal coil, these detectors together achieve a transverse momentum resolution of $\delta p_t/p_t = 6 \times 10^{-4} p_t \oplus 5 \times 10^{-3}$ (p_t in GeV/c).

The excellent resolution of the silicon microstrip detector facilitates the identification of jets containing b hadrons. A neural network combines impact parameter and secondary vertex information with other jet information such as track multiplicity, track rapidity, and the presence of leptons, to provide a measure of the b content of jets.

An electromagnetic calorimeter placed between the TPC and the superconducting coil identifies electrons and photons, and measures their energies with a resolution of $\delta E/E = 0.18/\sqrt{E} + 0.009$ (E in GeV). This sampling calorimeter has a depth of 22 radiation lengths and consists of projective towers each of which subtends a solid angle of approximately $0.9° \times 0.9°$.

The iron return yoke is instrumented with 23 layers of streamer tubes and serves as a hadronic calorimeter. It is seven interaction lengths deep and achieves an energy resolution of $\delta E/E = 0.85/\sqrt{E}$ for charged and neutral hadrons. Two additional layers of streamer tubes outside the return yoke aid the identification of muons.

The luminosity is measured with small-angle Bhabha events, using lead-proportional wire sampling calorimeters [3], with an accepted Bhabha cross section of 4.6 nb at 182.7 GeV and 4.3 nb at 188.6 GeV [4]. Integrated luminosities of 56.81 ± 0.11 (stat.) ± 0.29 (syst.) pb^{-1} and 174.21 ± 0.20 (stat.) ± 0.82 (syst.) pb^{-1} were recorded respectively, at mean centre-of-mass energies of 182.66 ± 0.05 GeV and 188.63 ± 0.04 GeV [5].

An energy flow algorithm [2] combines the information from the tracking detectors and calorimeters and provides a list of reconstructed charged and neutral particles. These energy flow objects are used in the analysis described below.
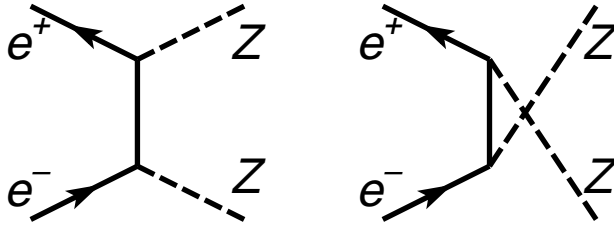
Figure 1: The *t*-channel exchange diagrams show the e$^+$e$^-$ → ZZ $\mathcal{NC2}$ processes in the Standard Model.

3 Simulation of Signal and Background

The YFSZZ Monte Carlo generator [6] provides a calculation of the expected Standard Model cross section for the $\mathcal{NC2}$ processes. The expected cross section is 0.26 pb at $\sqrt{s}$ = 182.7 GeV and 0.65 pb at 188.6 GeV. With a consistent set of electroweak parameters, three other Monte Carlo generators—PYTHIA [7], EXCALIBUR [8], and GRACE4F [9]—all agree with the YFSZZ calculation within 2%. This value is taken as the theoretical uncertainty on the $\mathcal{NC2}$ cross section determination.

Samples of ZZ compatible events from the $\mathcal{NC2}$ and $\mathcal{NC8}$ diagrams were generated with the PYTHIA Monte Carlo generator. The efficiencies were determined from the $\mathcal{NC2}$ sample. The $\mathcal{NC8}$ diagrams include, in addition to the diagrams of Figure 1, six other diagrams in which one or both Z bosons are replaced by a virtual photon. The difference between the $\mathcal{NC2}$ sample and the $\mathcal{NC8}$ sample was taken as background. This procedure accounts for any interference between the four-fermion diagrams. As a check, the analysis was repeated with samples generated with the EXCALIBUR Monte Carlo generator (see Section 6.1).

The KORALW [10] Monte Carlo generator was used to create a sample of WW-like four-fermion background events. To avoid double counting, events in the $\mathcal{NC8}$ ZZ sample with a WW-like final state are removed. As the KORALW generator does not include the part of the e$^+$e$^-$ → Weν and e$^+$e$^-$ → Ze$^+$e$^-$ processes with an electron near the beam axis and outside of the detector fiducial volume, additional samples for these processes were generated with the PYTHIA Monte Carlo generator.

For the two-fermion background, e$^+$e$^-$ → $\mu^+\mu^-$ and e$^+$e$^-$ → $\tau^+\tau^-$ events were generated with KORALZ [11], e$^+$e$^-$ → e$^+$e$^-$ events with BHWIDE [12], and e$^+$e$^-$ → q$\overline{\text{q}}$ events with PYTHIA. The two-photon background—$\gamma\gamma$ → e$^+$e$^-$, $\gamma\gamma$ → $\mu^+\mu^-$, and $\gamma\gamma$ → $\tau^+\tau^-$—was generated with PHOT02 [13]. Studies showed that the process $\gamma\gamma$ → hadrons contributes negligibly to the background expectation after all of the analysis cuts.

Table 1: The efficiencies, ZZ signal expectation, background expectation, number of observed events, and the measured $\mathcal{NC2}$ cross section with the statistical error for each channel at $\sqrt{s} = 188.6$ GeV.

	ϵ (%)	$N_{\mathrm{ZZ}}^{\mathrm{SM}}$	N_{bkg}	N_{obs}	σ_{ZZ} (pb)
$\ell\ell\mathrm{XX}^{\ddagger}$	76.7±0.5	8.8	1.1±0.3	12	$0.80\pm^{0.28}_{0.23}$
$\mathrm{q\bar{q}q\bar{q}}$ (b)*	14.6±0.2	8.3	3.8±0.4	14	$0.80\pm^{0.32}_{0.27}$
$\mathrm{q\bar{q}q\bar{q}}$ (non-b)*	27.4±0.2	16.0	60.0±1.4	69	$0.36\pm^{0.35}_{0.32}$
$\mathrm{q\bar{q}q\bar{q}}^{\dagger}$	31.5±1.2	17.2	19.7±1.8	32	$0.58\pm^{0.22}_{0.19}$
$\mathrm{q\bar{q}}\nu\bar{\nu}$*	47.2±0.3	15.0	13.0±0.6	30	$0.74\pm^{0.25}_{0.22}$
$\mathrm{q\bar{q}}\nu\bar{\nu}^{\dagger}$	79.8±0.7	25.3	64.5±1.6	88	$0.65\pm^{0.22}_{0.20}$
$\ell\ell\nu\bar{\nu}^{\ddagger}$	50.3±1.5	1.4	1.5±0.3	1	$-0.26\pm^{0.66}_{0.30}$
$\tau\tau\mathrm{q\bar{q}}^{\dagger}$	42.2±1.3	2.2	1.5±0.2	3	$0.44\pm^{0.62}_{0.41}$

* cut analysis   † NN analysis   ‡ both analyses

4 Event Selection

The analyses described below select events from all visible ZZ final states. While based on the Higgs boson search [14], these analyses have been tailored to the ZZ production process.

Two parallel analyses measure the ZZ production cross section. The first is an entirely cut-based analysis which uses the $\mathrm{q\bar{q}q\bar{q}}$, $\mathrm{q\bar{q}}\nu\bar{\nu}$, $\ell\ell\mathrm{XX}$, and $\ell\ell\nu\bar{\nu}$ channels. Throughout this paper, the symbol ℓ denotes an electron or muon and X denotes a quark or charged lepton. The second analysis, the "NN" analysis, replaces the cut-based selections in the $\mathrm{q\bar{q}q\bar{q}}$ and $\mathrm{q\bar{q}}\nu\bar{\nu}$ channels with neutral networks and introduces an additional neural network to identify the $\tau\tau\mathrm{q\bar{q}}$ final state.

Table 1 summarizes the results of the selections described below.

4.1 Selection of ZZ $\to \ell\ell$XX Final States

This analysis identifies those events in which one of the Z bosons decays into a pair of electrons or muons and the other decays into anything except neutrinos. Although the branching fraction of Z $\to \ell\ell$ is small, the analysis benefits greatly from the high lepton identification efficiency and excellent mass resolution.

Selected events have four or more reconstructed charged particles. The total energy of all the charged particles must exceed 10% of the centre-of-mass energy. To remove radiative returns to the Z, the most energetic isolated photon in an event must have an energy less than $0.75\,\gamma_{\mathrm{peak}}$, where γ_{peak} is the most likely energy of the radiative return photon and is given by $\gamma_{\mathrm{peak}} = 0.5\,(\sqrt{s} - m_{\mathrm{Z}}^2/\sqrt{s})$.

Standard lepton cuts are used to identify electrons and muons in the event [15]. Electron energies are corrected for possible bremsstrahlung losses. To maintain a high selection efficiency, isolated charged particles are also considered as lepton candidates. The isolation is defined as the half-angle of the largest cone about a particle's direction

which contains 5% or less of the event's total energy. Isolated particles have an isolation angle greater than 10°. The pair of oppositely-charged lepton candidates with an invariant mass closest to the Z mass is chosen as the Z → ℓℓ pair. Only those pairs with at least one identified lepton are considered and $e\mu$ combinations are rejected. Photons consistent with final state radiation are included in the calculation of the invariant mass of the lepton pair. Events in which the lepton pair contains an electron consistent with one from a photon conversion are rejected.

After the Z → ℓℓ lepton pair has been selected, the DURHAM algorithm [16] clusters the remainder of the event into two jets; these jets must contain at least one charged particle. To remove Zγ^* events, the selection requires that the invariant mass of the two jets exceed 15 GeV/c^2. To remove q$\overline{\text{q}}$ events, the sum of the transverse momenta of the leptons with respect to the nearest jet must be greater than 20 GeV/c, where the nearest jet is the one which forms the smallest invariant mass with the lepton.

The process WW → q$\overline{\text{q}}\ell\nu$ constitutes a large background for the selected events in which the Z → ℓℓ pair contains one identified lepton and one isolated charged particle. The two W masses are calculated assuming that the event comes from this process. The mass m_{lep} is the invariant mass of the identified lepton and the missing momentum; the other mass m_{had} is the invariant mass of the remainder of the event. For selected events, these masses satisfy either $m_{\text{had}} + m_{\text{lep}} < 150$ GeV/c^2 or $m_{\text{had}} - m_{\text{lep}} > 20$ GeV/c^2.

The mass of the lepton pair is used as the mass of the first Z candidate; that of the second candidate is the mass recoiling against the two leptons. Requiring the above cuts and that both Z masses be larger than 30 GeV/c^2, the analysis selects 92 events from the data with 90.6 ± 1.4 expected from signal plus background. Figure 2 shows the dilepton invariant mass distribution.

To further reduce background levels, the two reconstructed masses must be consistent with the Z boson mass. As the leptonic invariant mass and recoil mass have different resolutions, an elliptical cut is defined using

$$r^2 = \left(\frac{m_{\ell\ell} - m_{\text{Z}}}{\sigma_{m_{\ell\ell}}}\right)^2 + \left(\frac{m_{\text{recoil}} - m_{\text{Z}}}{\sigma_{m_{\text{recoil}}}}\right)^2,$$

where $\sigma_{m_{\ell\ell}} = 2.5$ GeV/c^2 and $\sigma_{m_{\text{recoil}}} = 3.3$ GeV/c^2. Selected events have $r < 3$. An ℓℓXX candidate, classified as a ZZ → $\mu\mu\tau\tau$ event, is shown in Figure 3.

Systematic uncertainties from lepton identification, tracking resolutions, and reconstruction of kinematic variables have been studied. The total relative systematic uncertainty on the efficiency is 1.3% and the relative uncertainty on the expected number of background events is 27%. Both uncertainties are dominated by limited Monte Carlo statistics.

4.2   Selection of ZZ → q$\overline{\text{q}}$q$\overline{\text{q}}$ Final States

A total reconstructed energy near $\sqrt{s}$ and four distinct jets characterize events from the ZZ → q$\overline{\text{q}}$q$\overline{\text{q}}$ final state. This final state has the largest branching fraction, but also the largest background.

The cut-based and NN-based analyses of this channel use a common preselection. The event must contain eight or more charged particles and the total energy of all charged
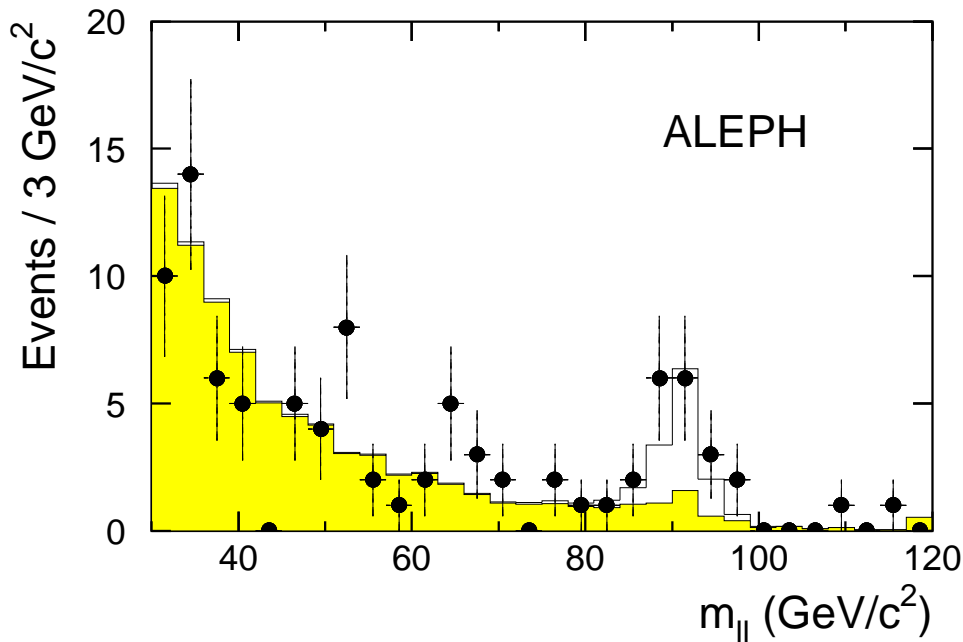
Figure 2: The distribution of the dilepton masses for the $\ell\ell$XX channel. All cuts except the elliptical mass cut have been applied. The grey histogram shows the expected background and the hollow histogram shows the expected signal.

particles must exceed 10% of the centre-of-mass energy.

The DURHAM algorithm clusters the event into four jets. To remove those events inconsistent with a four-jet topology, the value of y_{34}, the $y_{\rm cut}$ in the clustering algorithm which changes the event from a three-jet to four-jet topology, must be larger than 0.004. Additionally, each jet must contain at least one charged track.

Two additional cuts suppress events with initial state radiation. First, the longitudinal momentum of the event must satisfy the requirement $|p_z| < 1.5\,(M_{\rm vis} - 90)$ with $M_{\rm vis}$ in GeV/c^2 and p_z in GeV/c, to remove events in which the initial state photon is along the beam axis and outside of the detector fiducial volume. Second, the electromagnetic fraction of all of the jets must be smaller than 80% to remove those events in which the photon is inside the fiducial volume. This second cut also removes the $q\bar{q}e^+e^-$ overlap with the leptonic channel described above.

4.2.1 Cut-based Selection

The cut analysis tightens the preselection with three additional cuts. The first two target $q\bar{q}$ events: the thrust value of the event must be smaller than 0.9 and the sum of the four smallest angles between jets must be greater than 350°. The third cut reduces the overlap of $q\bar{q}\mu^+\mu^-$ events between the $q\bar{q}q\bar{q}$ and the $\ell\ell$XX selections. Accepted events have an invariant mass of the two most energetic muon candidates $m_{\mu\mu}$ less than 50 GeV/c^2 and satisfy the condition $p_1 + p_2 - m_{\mu\mu}c < 35$ GeV/c, where p_1 and p_2 are the momenta of the two muons. For events with only one identified muon, this cut reduces to $p_1 < 35$ GeV/c.
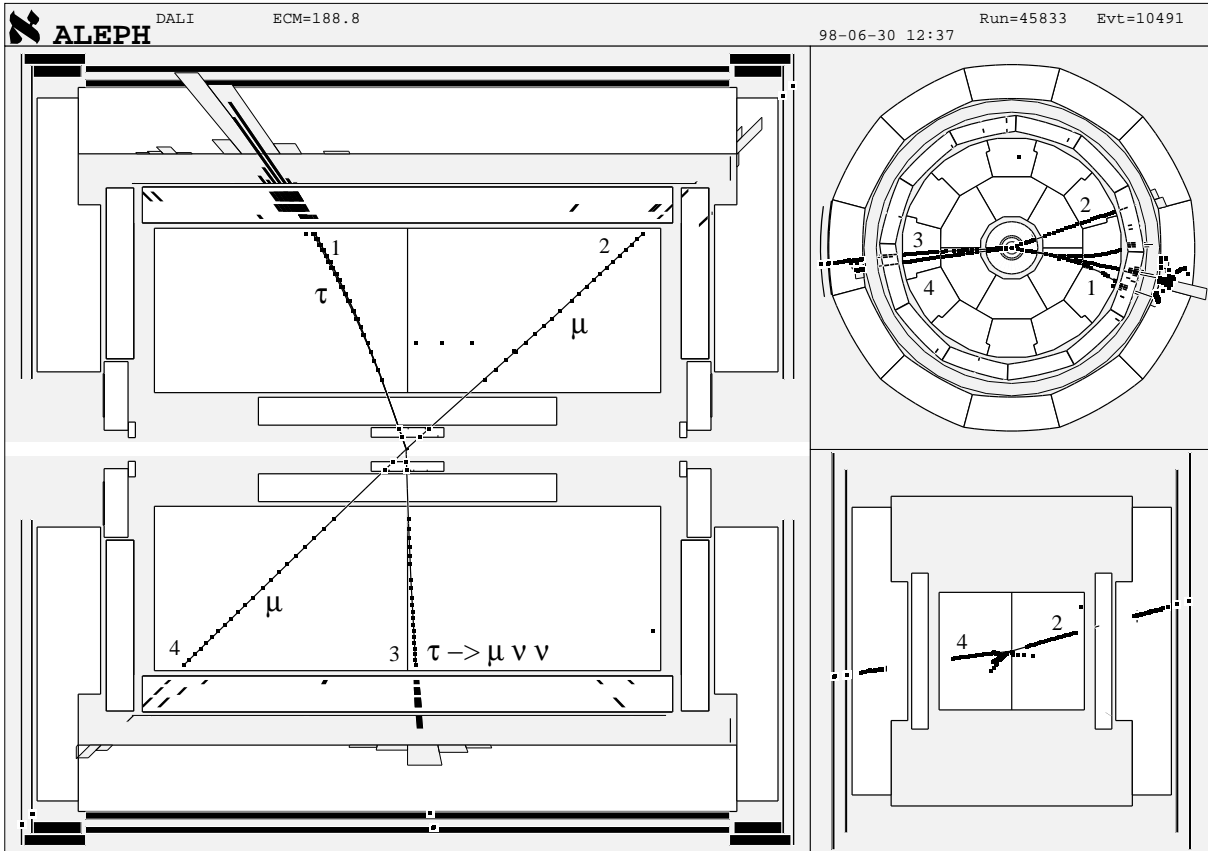
Figure 3: An event selected by the $\ell\ell XX$ analysis and classified as a ZZ $\to \mu\mu\,\tau\tau$ candidate. Tracks 2 and 4 form the Z $\to \mu\mu$ candidate with an invariant mass of 96.0 GeV/c^2. Tracks 1 and 3 form the Z $\to \tau\tau$ candidate with a recoil mass of 90.3 GeV/c^2.

These negligibly affect the efficiency for the q$\overline{q}$q$\overline{q}$ final state but reject more than 97% of the q$\overline{q}\mu^+\mu^-$ overlap and also a small fraction of the WW background.

After the above preselection, 1352 ± 6 events are expected from the simulation, approximately 80% of which are WW $\to$ q$\overline{q}$q$\overline{q}$ events. In the data, 1219 events are observed. This discrepancy has already been reported by ALEPH in a preliminary measurement of the WW $\to$ q$\overline{q}$q$\overline{q}$ cross section [17]. Its impact on the ZZ cross section measurement is studied in Section 6.2.

The selection subsequently relies on the tagging of jets from b quarks and on the dijet mass information. A four-constraint fit [18] is then applied to improve the jet momentum resolution. A b-tagging neural network produces a value η_i for each jet which is near unity for b jets and near zero for other jets [14].

The four-jet analysis is split into three sub-analyses: a b$\overline{b}$b$\overline{b}$ selection, a b$\overline{b}$q$\overline{q}$ selection, and a non-b quark selection. When calculating the cross section, the two b selections are treated as a single channel. The last sub-analysis replaces the b-tagging cuts with strict mass requirements to reject background while retaining efficiency for the majority of ZZ events ($\sim$62%) which do not contain b quark jets.

The b$\overline{b}$b$\overline{b}$ analysis selects events with high b content, well-isolated jets, and large dijet

masses. It requires that $y_{34} > 0.020$, that the sum of the dijet masses for at least one of the dijet combinations be above 170 GeV/c^2, and that $9.5\,y_{34} + \sum \eta_i > 3.1$ where the sum is over the four reconstructed jets.

For the other sub-selections the b-tagging requirements give way to tighter dijet mass requirements. The mass information is contained in the quantities χ_{W} and χ_{Z} defined as

$$\chi_i^2 = \left(\frac{m_{12} + m_{34} - 2\,m_i}{\sigma_S^i}\right)^2 + \left(\frac{m_{12} - m_{34}}{\sigma_D^i}\right)^2 ,$$

where i stands for W or Z. The quantities σ_S^i and σ_D^i are the resolutions of the sum and the difference of the dijet masses for the correct dijet combination, respectively. The contours of constant χ_{W} and χ_{Z} define two ellipses referred to as WW and ZZ ellipses throughout this section. For the WW and ZZ ellipses respectively, the values 4 and 3 GeV/c^2 are used for σ_S^i and the values 10 and 16 GeV/c^2, for σ_D^i.

The $b\bar{b}q\bar{q}$ selection requires that at least one dijet combination falls inside the ZZ ellipse with $\chi_{\mathrm{Z}} < 2.40$. For that combination, the dijet not containing the most poorly b-tagged jet must be compatible with $\mathrm{Z} \to b\bar{b}$ in terms of b-tagging: $\min(\eta_1, \eta_2) > 0.20$ and $-\log_{10}(1 - \eta_1)(1 - \eta_2) > 1.50$.

Finally, the selection for $q\bar{q}q\bar{q}$ events without b jets raises the y_{34} cut to 0.006, tightens further the ZZ ellipse to $\chi_{\mathrm{Z}} < 1.75$, and reduces the WW background by requiring that no dijet combination falls inside a WW ellipse with $\chi_{\mathrm{W}} < 1.60$. To maintain the statistical independence of the b and non-b selections, this selection accepts only those events which have not been previously selected by the $b\bar{b}b\bar{b}$ or $b\bar{b}q\bar{q}$ cuts.

Figure 4 shows the sum of the dijet masses for the $b\bar{b}b\bar{b}$ and $b\bar{b}q\bar{q}$ selections with the elliptical mass cut removed.

Although this selection does not specifically target $\tau\tau q\bar{q}$ events, it nonetheless has a significant efficiency for these events ($\sim$17%). Consequently, the $\tau\tau q\bar{q}$ selection described below is not included in the cut-based cross section measurement.

4.2.2 Neural Network Selection

A multivariate neural network is trained to select ZZ signal events from $q\bar{q}$ and WW background events. During training, the network is presented with up to six dijet combinations per $q\bar{q}$ or WW event, but only the correct dijet pairing for each signal event. If one Z boson decays to b quarks, those jets are labelled 3 and 4, and the other two jets are labelled 1 and 2. Otherwise the jet labels are random. Reconstructed dijet masses are obtained using a four-constraint fit which requires energy-momentum conservation. Twenty-three event variables are used to discriminate specific signal and background features. In many cases, inclusion of similar variables in different combinations improves the neural network training.

The event variables y_{34}, thrust, and sphericity aid in selecting events with four separated jets. The missing energy and $\max(E_{\mathrm{charged\ track}}/E_{\mathrm{jet}})$, the maximum scaled energy among all jets of the most energetic charged track in a jet, specifically reject semileptonic W decays.

A b-tagging neural network [14] gives an output η_i for each jet, and these variables are input as $\min(\eta_3, \eta_4)$, $(1 - \eta_3)(1 - \eta_4)$, and $\sum_{i=1}^4 \eta_i$.
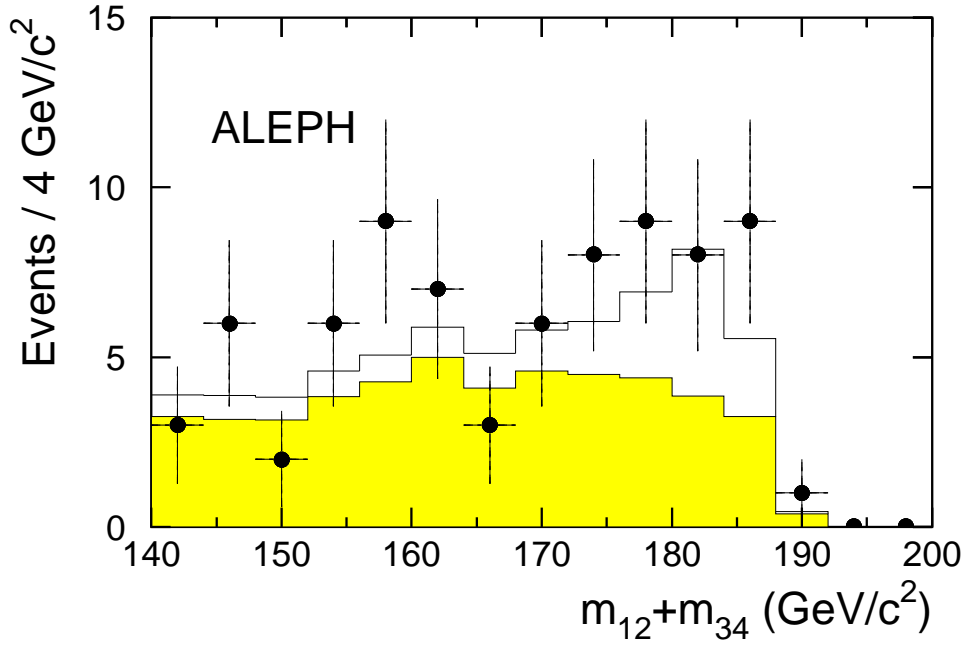
Figure 4: The distribution of the sum of the dijet masses $(m_{12} + m_{34})$ for the $b\bar{b}b\bar{b}$ and $b\bar{b}q\bar{q}$ channels. All cuts have been applied except the elliptical mass cut. The hollow histogram is the contribution from the signal and the darker region that from the expected background.

The reconstructed dijet masses aid the selection of resonant ZZ production events. The mass combinations used as network inputs are m_{12}, m_{34}, and $(m_{12} - m_{34})^2 + (m_{34} - m_Z)^2$. These variables perform the same function as an elliptical mass cut.

The jet boosted sphericity (calculated in the rest frame of the jet) of the two jets with lowest η_i, the track multiplicity in these jets, and the two lowest jet masses all help to separate light quark jets from gluon jets. The track multiplicity in this case is restricted to tracks with a rapidity with respect to the jet axis greater than 1.6.

The sum of the four smallest inter-jet angles discriminates against $q\bar{q}$ background events. The angular variable $\min\left(\cos\theta_{ij} + \cos\theta_{kl}\right)$ minimized over all jet combinations selects events with pairs of back-to-back jets. The event broadening variable $B = \min(B_+, B_-)$ also aids in this discrimination by rejecting $q\bar{q}$ background with gluons that can lead to broad jets. The broadening variable for each of the two hemispheres $S_\pm$ is given by $B_\pm = (\sum_{i \in S_\pm} p_{Ti})/(\sum_i |p_i|)$, where p_T is calculated with respect to the thrust axis and the sums run over tracks. Finally, the largest jet energy and the two smallest jet energies improve the overall discriminating power.

Of all of the dijet combinations, the one with the largest neural network output is used. The output of the neural network is shown in Figure 5 for Monte Carlo simulation and for data. Only events with a network output greater than 0.7 are used in the cross section calculation.
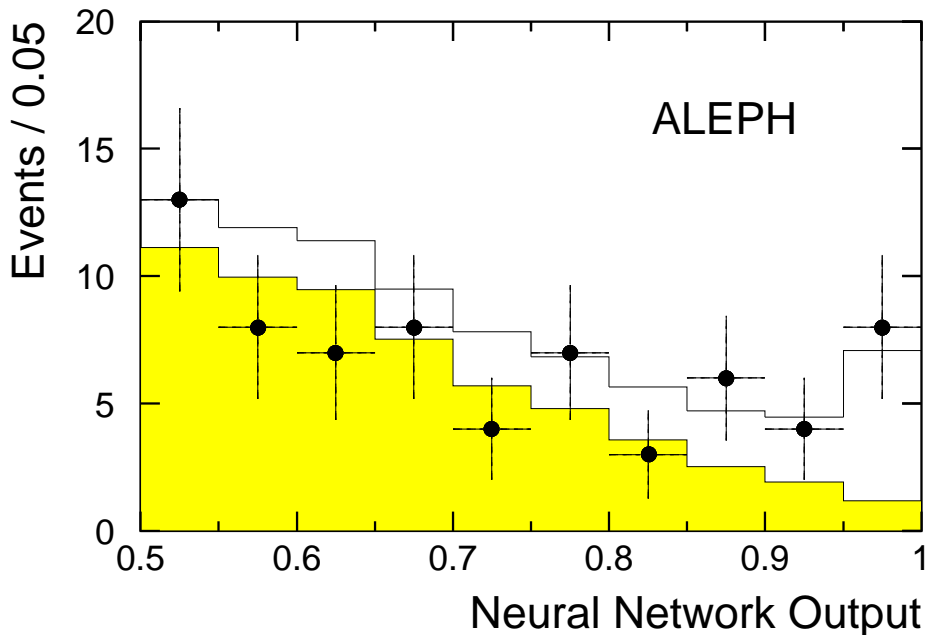
Figure 5: Neural network output from the q$\overline{q}$q$\overline{q}$ selection for data and Monte Carlo simulation. The grey histogram shows the expected background, and the hollow histogram shows the expected $\mathcal{NC2}$ signal.

4.2.3 Systematic Uncertainties

The systematic uncertainties in this channel include effects from the modelling of b physics, from discrepancies in tracking between the simulation and the data, from discrepancies in reconstructed jet kinematics, from uncertainties in the background cross sections, and from uncertainties in gluon splitting into heavy flavours.

For the cut-based analysis, the total relative systematic uncertainties on the signal efficiencies are 1.7% and 1.3% for the b and non-b selections, respectively, with all of the sources having comparable contributions. The relative uncertainties for the background are 13% and 4%, dominated by the limited Monte Carlo statistics and jet corrections.

For the NN-based analysis, the total relative systematic uncertainty on the signal efficiency is 3%. No single effect dominates the uncertainty. The total relative uncertainties for the background are 11% (q$\overline{q}$) and 7% (WW), dominated by uncertainties in the reconstruction of kinematic variables and limited Monte Carlo statistics.

4.3 Selection of ZZ → q$\overline{q}\nu\overline{\nu}$ Final States

Approximately 30% of the ZZ events have a q$\overline{q}\nu\overline{\nu}$ final state characterized by a missing mass $\displaystyle{\not}M$ and visible mass consistent with the Z mass.

Both the cut-based and NN-based analyses for this channel share a common preselection. Events must contain more than four reconstructed charged particles and the total energy of all the charged particles must exceed 10% of the centre-of-mass energy. The plane perpendicular to the thrust axis divides the event into two hemispheres. These
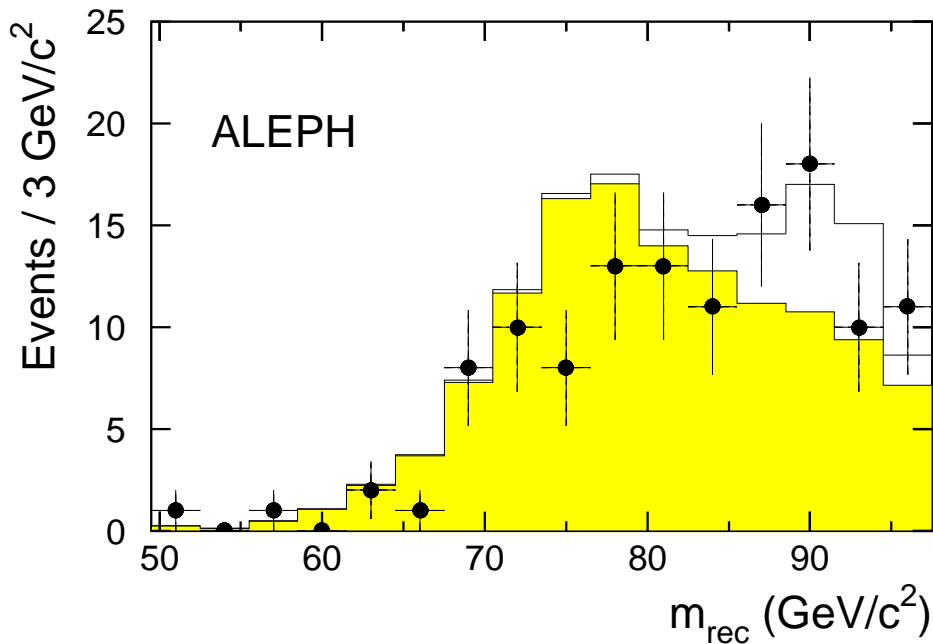
9

Figure 6: The distribution of reconstructed masses for the $q\bar{q}\nu\bar{\nu}$ channel. The grey region is the expected contribution from the background and the hollow region that from the ZZ $\mathcal{NC}2$ signal.

hemispheres are the "jets" used to calculate all of the kinematic quantities below. Both of the hemispheres must have a nonzero energy.

The preselection rejects events with a total energy more than 30° degrees from the beam axis smaller than $0.25\sqrt{s}$ and a missing transverse momentum smaller than $0.05\sqrt{s}$. This cut primarily removes $\gamma\gamma \rightarrow$ hadrons events.

Two additional cuts remove much of the background from $q\bar{q}$ events with initial state radiation. First, the magnitude of the longitudinal event momentum must be less than 50 GeV/c. Secondly, the missing mass must be greater than 50 GeV/c^2.

After the preselection, the background is dominated by $q\bar{q}$ and WW events. Assuming the Standard Model cross section for ZZ production, 1533 ± 7 events are expected in good agreement with the 1493 actually observed in the data.

4.3.1 Cut-based Selection

The two-fermion background remaining after the preselection consists largely of $q\bar{q}$ events with two or more initial state radiative photons. Requiring the acoplanarity A_{12} to be greater than 0.08 removes much of this background. The acoplanarity of the two jets is $A_{12} = (\hat{j}_1 \times \hat{j}_2) \cdot \hat{z}$ where $\hat{j}_i$ are the unit vectors along the jet directions.

Pairs of W bosons which subsequently decay as WW $\rightarrow \tau\nu\,q\bar{q}$ form the other major background. To reject cases where the tau lepton decays leptonically, a cut on the isolation of identified leptons is made. The isolation is defined as the sum of the energy in a 30° cone around the lepton direction. Selected events have an isolation greater than 13 GeV.

When the lepton from the tau decay is unidentified or the tau lepton decays hadronically, the previous cut is ineffective. To remove these cases, the analysis requires that the angle between the reconstructed charged particle with the highest momentum and the nearest charged particle be less than 20°. Additionally, the event is reclustered into minijets with the JADE algorithm [19] using $y_{\text{cut}} = (2 \text{ GeV}/\sqrt{s})^2$. The energy of the most isolated minijet must be smaller than 8 GeV.

To remove events from the $e^+e^- \rightarrow We\nu$ and $e^+e^- \rightarrow Ze^+e^-$ processes which have a detected final state electron near the beam axis, the analysis requires that the energy in a cone of 12° around the beam axis must be smaller than $0.02\sqrt{s}$. To remove events which have a missing momentum near the beam axis and may be poorly measured, the smallest angle between the missing momentum and the beam axis must be larger than 25°. Figure 6 shows the distribution of the reconstructed mass for candidates which pass all of the above cuts. The reconstructed mass m_{rec} is the invariant mass of the two jets calculated with the missing mass constrained to m_Z.

Because the mass of the Z boson is known, the mass information can be used effectively to reject much of the background. As for the other channels, this selection uses an elliptical mass cut of "radius"

$$r^2 = \left(\frac{m_{\text{rec}} - m_Z}{\sigma_{m_{\text{rec}}}}\right)^2 + \left(\frac{M\!\!\!/ - m_Z}{\sigma_{M\!\!\!/}}\right)^2,$$

where $\sigma_{m_{\text{rec}}} = 3.1 \text{ GeV}/c^2$ and $\sigma_{M\!\!\!/} = 8.5 \text{ GeV}/c^2$ are the resolutions. Selected events have $r < 2$.

4.3.2 Neural Network Selection

After preselection, a 12-variable neural network is employed to distinguish signal events from background. Four of the variables used in the neural network analysis (acoplanarity, minijet energy, direction of missing momentum, and energy within a 12° cone around the beam axis) are shared with the cut analysis. Additionally, the neural network analysis uses the reconstructed Z boson mass and the missing mass directly rather than using an elliptical mass cut. This analysis also includes two b-tagging variables although only a small fraction of events have a $b\overline{b}\nu\overline{\nu}$ final state. In addition, acollinearity, the visible energy beyond 30° of the beam axis, the energy within a 30° wedge of the direction of the missing momentum, and the z-component of the momentum are used as variables. The output of the neural network is shown in Figure 7 for Monte Carlo simulation and for data. Only events with a network output greater than 0.5 are used for the cross section calculation.

4.3.3 Systematic Uncertainties

The results have been corrected for unsimulated accelerator background events which increase the energy deposited near the beam axis; this effect was studied using random triggers. In addition, half of the correction is used as an estimate of the systematic uncertainty. Similarly, the jet kinematics are corrected to make them correspond better to those observed in the data. Again, half of this correction is used as the systematic uncertainty. The systematic uncertainties also include uncertainties from the background production cross sections and the limited statistics of the Monte Carlo samples.
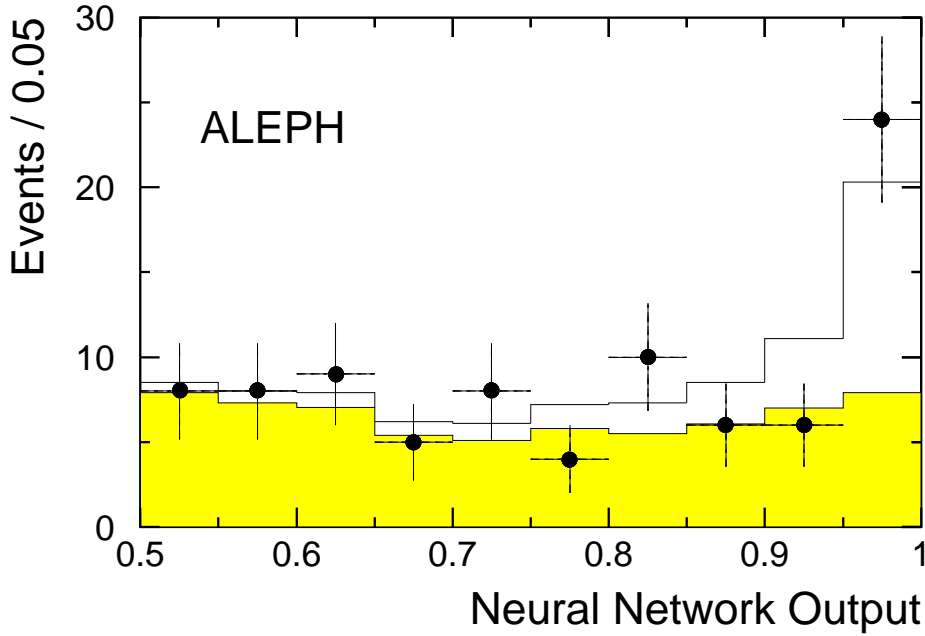
Figure 7: Neural network output from the q$\bar{\text{q}}\nu\bar{\nu}$ selection for data and Monte Carlo simulation. The grey histogram shows the expected background, and the hollow histogram shows the expected $\mathcal{NC2}$ signal.

Adding these uncertainties in quadrature gives total relative uncertainties of 2% and 5% on the signal and background, respectively, for the cut-based analysis. For the efficiency, all of the sources are significant; for the background, the limited Monte Carlo statistics dominate.

For the NN-based analysis, the b-tagging systematic uncertainties are estimated by reweighting the data with a function obtained from comparison of Z-peak Monte Carlo simulation and data. The relative systematic errors on signal and background are 2% and 3%, respectively.

4.4 Selection of ZZ $\to \ell\ell\nu\bar{\nu}$ Final States

The preselection requires events to have exactly two identified electrons or muons and no other reconstructed charged particles. These leptons must have the same flavour and opposite charge. The fraction of the centre-of-mass energy deposited in the detector more than 30° from the beam axis $f_{30°}$ must satisfy the requirement $0.4 < f_{30°} < 0.6$. The angle between the two lepton directions must be less than 178°. For electron pair events, 49 ± 2 events are expected and 43 observed; for muon pair events, 13.2 ± 0.3 events are expected and 10 observed.

Cuts on other kinematic quantities further suppress the background. The invariant mass of the leptons and the missing mass are required to be within an ellipse of $r < 1.7$ defined as above with $\sigma_{\not{M}} = 3.3$ GeV/c^2 and $\sigma_{m_{\ell\ell}} = 2.5$ GeV/c^2. The angle between the missing momentum and the beam axis must be larger than 6.7°, and the total energy not

associated with the leptons must be less than 5.6 GeV.

The systematic uncertainty is 5% for the efficiency and 17% for the background. These include uncertainties from lepton identification and tracking resolution but are dominated by the limited Monte Carlo statistics.

4.5 Selection of ZZ → ττqq̄ Final States

In the neural network based selection, a dedicated analysis selects ZZ → ττqq̄ events with a higher efficiency than the cut-based four-jet selection.

Events must contain at least eight tracks and the total energy of all the charged particles must exceed $0.20\sqrt{s}$. Background from WW and ZZ events with electron or muon decays is suppressed by rejecting events having an identified lepton with energy greater than $0.25\sqrt{s}$. Radiative returns to the Z peak, characterized by high missing energy and high missing longitudinal momentum, are rejected by requiring $|p_z| + \not{E} < 1.8\,\gamma_{\mathrm{peak}}$, where p_z and $\not{E}$ are respectively the missing longitudinal momentum and missing energy. To further reject radiative returns, events are also rejected if the event $|p_z|$ is greater than $0.6\,\gamma_{\mathrm{peak}}$.

Events passing the preselection cuts are clustered into minijets having invariant masses consistent with a tau lepton, $m_{\mathrm{jet}} < 2.7$ GeV/c^2. The τ candidates are selected from these minijets using a series of quality cuts based on multiplicity, isolation, and momentum. To be considered a τ candidate, a minijet must have one, two, or three charged tracks with momenta larger than 1 GeV/c. If the minijet has three charged tracks, it must be of unit charge; if the minijet has two charged tracks, the minijet charge is the charge of the track with higher momentum. The minijet isolation angle must be larger than 15°. This isolation angle is the half-angle of the largest cone around the minijet direction containing, in addition to the minijet energy, no more than 5% of the total event energy outside the cone. Finally, the energy of a two- or three-prong minijet must be greater than 12.5 GeV, while a one-prong minijet with less than 80% of its energy from charged particles must have an energy greater than 7.5 GeV. Otherwise, no momentum cut is made.

Only events with at least two τ candidates are further considered. At least one of the τ minijets must have exactly one prong, and the two minijets must have opposite charge. The rest of the event is clustered into two jets using the Durham algorithm. All four jets in the event are rescaled using an overconstrained kinematic consistency fit in which the jet directions are fixed and the minijet masses are set to m_τ. The fit χ^2 is calculated from energy-momentum conservation, the hadronic jet resolutions, and the difference between the two fitted dijet masses. This has the effect of constraining the dijets to equal masses. In no case are the hadronic jets allowed to rescale to less than 75% of their measured momenta. A typical event may have several possible combinations of potential τ minijet candidates; only the combination with the smallest calculated kinematic χ^2 is further considered.

A five-variable neural network selects ZZ events from preselected events. Because the τ leptons decay with one or two neutrinos, the event transverse momentum p_T is input to discriminate against background events without missing energy. The χ^2 provides a measure of the event's kinematic consistency with the ZZ signal. The sum of the τ candidates' isolation angles and the sum of the τ candidates' transverse momenta

with respect to their nearest hadronic jet distinguish τ minijets, which are expected to be well-isolated, from fake τ minijets on the periphery of a hadronic jet. Finally, the reconstructed Z mass, when combined with the implicit equal mass constraint, helps discriminate between $\mathcal{NC}2$ events and background. Events with a network output greater than 0.77 are selected for the cross section calculation.

The systematic uncertainties arise from uncertainties on the reconstructed jet energies and angles, the background cross sections, and the limited Monte Carlo statistics. The relative systematic errors for signal and background are 3.0% and 10.8%. The error for signal is distributed equally among the sources, while the background error is dominated by limited Monte Carlo statistics.

5 Combination of Channels

Table 1 summarizes the efficiencies, numbers of expected signal and background events, the number of observed events, and the measured cross section for each channel. A maximum likelihood fit determines the $\mathcal{NC}2$ cross section for the $e^+e^- \to ZZ$ process by combining the information from all of the channels.

For the cut-based analysis, only the total numbers of events are used in the likelihood combination. Overlaps between the various channels are less than 0.2% and are negligible.

For the given signal and background numbers, toy simulated experiments are generated, and the expected uncertainty on the cross section measurement is derived from the width of the extracted cross section distribution. The expected relative statistical uncertainty on the 188.6 GeV cross section measurement is 19.7%.

For the neural-network based analysis, a binned likelihood fit is used for the $q\overline{q}q\overline{q}$ and $q\overline{q}\nu\overline{\nu}$ channels where the shape of the neural-network distribution is used; for the other channels only the total numbers of events are used in the likelihood fit. The $q\overline{q}q\overline{q}$ distribution is divided into six bins between 0.7 and 1.0, while the $q\overline{q}\nu\overline{\nu}$ distribution is divided into ten bins between 0.5 and 1.0.

For the neural-network based analysis, the overlaps between channels are explicitly removed. About 0.2% of the events in the $q\overline{q}q\overline{q}$ selection are $\tau\tau q\overline{q}$ events in which a three-prong τ is misidentified as a quark jet, and about 0.5% are $q\overline{q}\mu^+\mu^-$ events. To ensure the exclusivity of the analyses, the overlapping signal and background are explicitly subtracted from the $q\overline{q}q\overline{q}$ results. The expected uncertainty after combining all channels is 18.0%.

The systematic uncertainties were determined by adding a Gaussian smearing to the efficiencies and background estimates in toy Monte Carlo experiments and observing the change in the total error. Correlated contributions to the total systematic uncertainty of the measurement include the luminosity (0.5%) and the uncertainties in the WW and $q\overline{q}$ cross sections. The total relative systematic uncertainties are 4% and 6% for the cut-based and neural-network based analyses, respectively.

The measured cross sections at $\sqrt{s} = 188.6$ GeV are

$$\sigma_{\mathrm{ZZ}} = 0.69 \pm {}^{0.13}_{0.12}\,(\mathrm{stat.}) \pm 0.03\,(\mathrm{syst.})\,\mathrm{pb}$$

and

$$\sigma_{\mathrm{ZZ}} = 0.64 \pm {}^{0.12}_{0.11}\,(\mathrm{stat.}) \pm 0.04\,(\mathrm{syst.})\,\mathrm{pb}$$
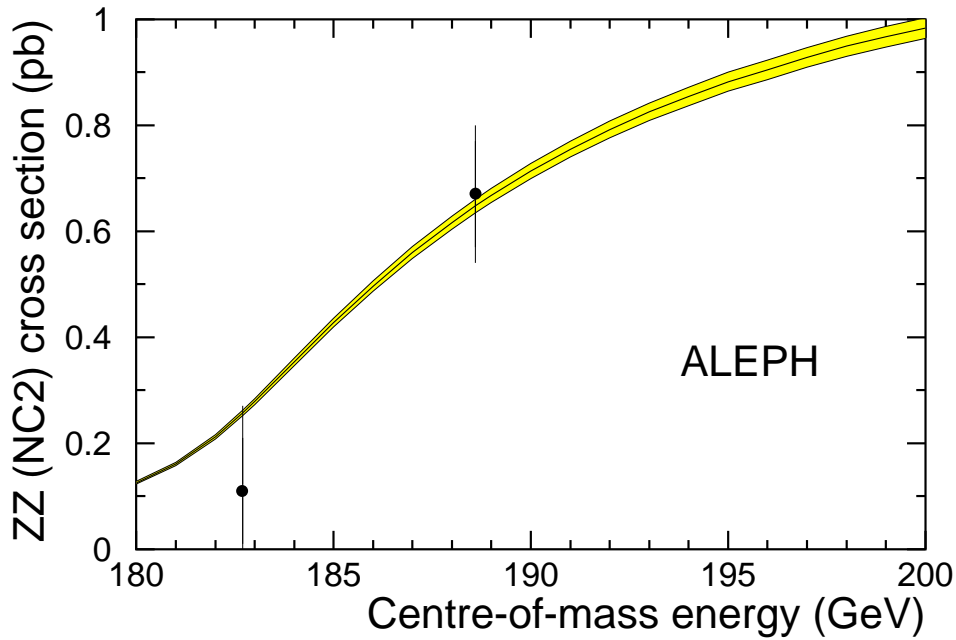
14

Figure 8: The measured $\mathcal{NC}2$ cross section as a function of the centre-of-mass energy compared to the expected Standard Model cross section. The shaded area represents the theoretical uncertainty (2%) on the YFSZZ calculations.

for the cut-based and neural-network based analyses, respectively, compared to the Standard Model expectation of 0.65 pb. Table 1 shows the cross section for each channel individually.

The cut-based analysis selects 13 candidates with an expected background of 12.2 events when applied to the 1997 data sample. The total efficiency for all channels is 33%. Combination of the channels with the above likelihood function yields a measured cross section of

$$\sigma_{\mathrm{ZZ}} = 0.11 \pm_{0.11}^{0.16}\,(\mathrm{stat.}) \pm 0.04\,(\mathrm{syst.})\,\mathrm{pb}$$

at a centre-of-mass energy of $\sqrt{s} = 182.7$ GeV, compared to the Standard Model expectation of 0.26 pb. The measurement is also consistent with a similar measurement from the L3 collaboration [20].

6 Cross Checks

6.1 Four-fermion Interference

The PYTHIA Monte Carlo generator does not fully simulate the interference between all of the four-fermion diagrams. This potentially biases the cross section measurement presented here. Using EXCALIBUR, which does include the interference, to generate samples for the signal and four-fermion background and rerunning the cut-based analysis yields a relative difference in the cross section measurement of -1%. This is a negligible

15

effect when compared to the magnitude of the statistical error.

6.2 Correlations Between the WW and ZZ Cross Sections

The preliminary measurement of the WW cross section in the $q\bar{q}q\bar{q}$ channel performed by ALEPH on the 1998 data differs from the Standard Model by -10%. Although this could be a statistical effect, the effect of a real reduction of the WW cross section on the extracted ZZ cross section was investigated. As a check, the expected WW background of the four-quark channels of the cut-based analysis was reduced by 10% and the channels recombined. This leads to a $+3.5\%$ relative change in the measured ZZ cross section.

7 Conclusions

Two analyses have measured the ZZ cross section using the data taken at $\sqrt{s} = 188.6$ GeV in 1998. The results agree and are consistent with the Standard Model expectation of 0.65 pb. The ZZ production cross section is taken to be the arithmetic average of the above two measurements

$$\sigma_{\text{ZZ}}(188.6 \text{ GeV}) = 0.67 \pm 0.13 \,(\text{stat.}) \pm 0.04 \,(\text{syst.}) \,\text{pb} \,.$$

Additionally, the cut-based analysis has been applied to the 1997 data sample yielding a measurement of

$$\sigma_{\text{ZZ}}(182.7 \text{ GeV}) = 0.11 \pm {}^{0.16}_{0.11} \,(\text{stat.}) \pm 0.04 \,(\text{syst.}) \,\text{pb} \,.$$

The measured cross section is compared to the Standard Model expectation in Figure 8.

Acknowledgements

The authors would like to thank W. Płaczek for his help with the YFSZZ generator. It is also a pleasure to congratulate our colleagues from the CERN accelerator divisions for the successful operation of LEP. We are indebted to the engineers and technicians in all our institutions for their contributions to the excellent performance of ALEPH. Those of us from non-member states thank CERN for its hospitality.

References

[1] ALEPH Collaboration (D. Decamp *et al.*), *"ALEPH: A Detector for electron-positron annihilations at LEP",* Nucl. Instrum. Methods **A294** (1990) 121.

[2] ALEPH Collaboration (D. Buskulic *et al.*), *"Performance of the ALEPH detector at LEP",* Nucl. Instrum. Methods **A360** (1995) 481; D. Creanza *et al., "Construction and performance of the new ALEPH vertex detector",* published in the Proceedings of the Conference on Advanced Technology and Particle Physics, Como, Italy (1996).

[3] ALEPH Collaboration (D. Decamp *et al.*), *"Measurement of the absolute luminosity with the ALEPH detector"*, Z. Phys. **C53** (1992) 375.

[4] S. Jadach *et al.*, *Analytical $\mathcal{O}(\alpha)$ distributions for Bhabha scattering at low angles"*, Phys. Lett. **B253** (1991) 469; S. Jadach, M. Skrzypek, and B.F.L. Ward, *"Is there a better way of exponentiating QED corrections?"* Phys. Lett. **B257** (1991) 173; S. Jadach *et al.*, *"Higher order QED corrections to Bhabha scattering at low angles"*, Phys. Lett. **B260** (1991) 438.

[5] The LEP Energy Working group (R. Assmann *et al.*), *"Evaluation of the LEP centre-of-mass energy for data taken in 1998"*, LEP Energy Working Group Note 99/01 available from http://www.cern.ch/LEPECAL/reports/reports.html.

[6] S. Jadach, W. Płaczek, and B.F.L. Ward, *"Gauge-invariant YFS exponentiation of (un)stable Z-pair production at and beyond CERN LEP2 energies"*, Phys. Rev. **D56** (1997) 6939.

[7] T. Sjöstrand, *"High-energy-physics event generation with PYTHIA 5.7 and JETSET 7.4"*, Comput. Phys. Commun. **82** (1994) 74.

[8] F.A. Berends, R. Pittau, and R. Kleiss, *"EXCALIBUR – A Monte Carlo program to evaluate all four-fermion processes at LEP 200 and beyond"*, Comput. Phys. Commun. **85** (1995) 437.

[9] T. Ishikawa *et al.*, *GRACE manual: automatic generation of tree amplitudes in standard models: version 1.0"*, KEK-92-19 (1993).

[10] M. Skrzypek *et al.*, *"Monte Carlo program KORALW 1.02 for W-pair production at LEP2/NLC energies with Yennie-Frautschi-Suura exponentiation"*, Comput. Phys. Commun. **94** (1996) 216.

[11] S. Jadach, B.F.L Ward, and Z. Wąs, *"The Monte Carlo program KORALZ version 4.0 for the lepton or quark pair production at LEP/SLC energies"*, Comput. Phys. Commun. **79** (1994) 503.

[12] S. Jadach, W. Płaczek, and B.F.L. Ward, *BHWIDE 1.00: $\mathcal{O}(\alpha)$ YFS exponentiated Monte Carlo for Bhabha scattering at wide angles for LEP1/SLC and LEP2"*, Phys. Lett. **B390** (1997) 298.

[13] J.A.M. Vermaseren, *"Two gamma physics versus one gamma physics and whatever lies inbetween"*, CERN-TH-2878 published in Proceedings of the IV International Workshop on Gamma Gamma Interactions, Amiens, France, eds. G. Cochard and P. Kessler (1980).

[14] ALEPH Collaboration, *"Search for the Neutral Higgs Bosons of the Standard Model and the MSSM in e^+e^- Collisions at $\sqrt{s} = 188.6$ GeV"*, ALEPH 99-007 (CONF 99-003) available from http://alephwww.cern.ch/; ALEPH Collaboration (R. Barate *et al.*), *"Search for the standard model Higgs boson at the LEP2 Collider near $\sqrt{s} = 183$ GeV"*, Phys. Lett. **B447** (1999) 336; *"Searches for the neutral Higgs*

17

bosons of the MSSM in the e⁺e⁻ *collisions at centre-of-mass energies of 181–184 GeV"*, Phys. Lett. **B440** (1998) 419, *erratum* Phys. Lett. **B447** (1999) 355.

[15] ALEPH Collaboration (D. Buskulic *et al.*), *"Heavy flavour production and decay with prompt leptons in the ALEPH detector"*, Z. Phys. **C62** (1994) 179.

[16] N. Brown and W.J. Stirling, *"Jet cross sections at leading double logarithm in* e⁺e⁻ *annihilation"*, Phys. Lett. **B252** (1990) 657; S. Catani *et al.*, *"New clustering algorithm for multijet cross sections in* e⁺e⁻ *annihilation"*, Phys. Lett. **B269** (1991) 432; N. Brown and W.J. Stirling, *"Finding jets and summing soft gluons: a new algorithm"*, Z. Phys. **C53** (1992) 629.

[17] ALEPH Collaboration *"WW cross section and W branching ratios at* $\sqrt{s}$ = 189 *GeV"*, ALEPH 99-020 (CONF 99-015), available from http://alephwww.cern.ch/.

[18] ALEPH Collaboration (R. Barate *et al.*), *"Measurement of the W mass in* e⁺e⁻ *collisions at* $\sqrt{s}$ = 189 *GeV"*, Phys. Lett. **B453** (1999) 121.

[19] JADE Collaboration, W. Bartel *et al.*, *"Experimental Studies on multijet production in* e⁺e⁻ *annihilation at PETRA energies"*, Z. Phys. **C33** (1986) 23; S. Bethke *et al.*, *"Experimental investigation of the energy dependence of the strong coupling strength"*, Phys. Lett. **B213** (1988) 235.

[20] L3 Collaboration, M. Acciarri *et al.*, *"Study of neutral current four fermion and* ZZ *production in* e⁺e⁻ *collisions at* $\sqrt{s}$ = 183 GeV", Phys. Lett. **B450** (1999) 281.